Electronic Supplementary Material (ESI) for Journal of Materials Chemistry A.

High thermoelectric performance in $XAgSe_2$ (X = Sc, Y) from strong quartic anharmonicity and multi-valley band structure

Xuhao Song,[1] Yinchang Zhao,[1,*] Jun Ni,[2] Sheng Meng,[3,4] and Zhenhong Dai[1,†]

[1]*Department of Physics, Yantai University, Yantai 264005, People's Republic of China*

[2]*Department of Physics, Tsinghua University, Beijing 100084, People's Republic of China*

[3]*Beijing National Laboratory for Condensed Matter Physics and Institute of Physics, Chinese Academy of Sciences, Beijing, 100190, People's Republic of China*

[4]*Collaborative Innovation Center of Quantum Matter, Beijing 100084, People's Republic of China*

(Dated: June 30, 2023)

Supplementary Methods

We conduct first-principles computations utilizing the Vienna Ab initio Simulation Package (VASP) software package[1], utilizing a plane-wave basis set and the projector augmented-wave (PAW)[2] technique to simulate the potentials of ion cores and valence electrons. The exchange-correlation interactions are addressed by employing the Perdew-Burke-Ernzerhof (PBE) functional[3] of the generalized gradient approximation (GGA). We select a kinetic energy cutoff of 500 eV and Γ-centered 13×13×8 k-point meshes to adequately sample the entire Brillouin zone. We establish a total energy convergence threshold of 10^{-8} eV, and a force criterion of 10^{-6} eV/Å for ion relaxation. The computed Born effective charge Z^* and permittivity ϵ, as per the density functional perturbation theory (DFPT)[4], are presented in Table S2, and are crucial for implementing non-analytical corrections in the dynamic matrix.

With the help of the ALAMODE code[5], we obtained the harmonic (second-order) interatomic force constants (IFCs) by applying a random displacement of 0.01 Å in the 2×2×2 supercell by the finite-displacement method[6]. Here, we also calculated the harmonic phonon dispersion curves within the 3×3×2 supercells to check the convergence of IFCs, as shown in Fig. S1(a). It can be observed that the harmonic phonon dispersion curves agree well with each other, indicating the harmonic IFCs exacted form the 2×2×2 supercell are enough to capture convergence results. Furthermore, it can be deduced that anharmonic IFCs exacted from 2×2×2 supercell are also convergent, since anharmonic IFCs generally converge faster than harmonic IFCs. To obtain the displacement and force datasets required for anharmonic (cubic and quartic) IFCs, we use 4000-step ab initio molecular dynamics (AIMD) simulation with 2 fs time step and 300 K temperature to capture 80 snapshots first. On this basis, we obtain 80 quasi-random configurations by applying the random displacement of 0.1 Å to each atom in the 80 snapshots. Finally, we extract displacement and force information obtained from 80 quasi-random configurations to derive anharmonic IFCs via the compressive sensing lattice dynamics (CSLD) method[7, 8]. In the CSLD calculations, we consider all (third-) nearest neighbor interactions for third- (fourth- to sixth-) order IFCs. Our calculations use 80 quasi-random configurations, more than used in previous work on Tl_3VSe_4[9] and cubic $SrTiO_3$[10], are sufficient to capture accurate aharmonic IFCs that produce convergent results.

We calculate the temperature-dependence anharmonic phonon energy eigenvalues, including the off-diagonal elements of phonon self-energies. On top of self-consistent phonon (SCP) theory calculations, the thermal transport parameters is solved based on the phonon Boltzmann transport equation (BTE), as employed in the FourPhonon package[11, 12]. Generally, the computational cost of four-phonon (4ph) scattering is expensive in most materials. Hence, to ensure sufficient convergence, we use the available 4ph phase spaces as the criterion for calculating the 4ph scattering rates. We use 13×13×8 q-mesh to capture the lattice thermal conductivity κ_L, and the numbers of available three-phonon (3ph) and 4ph scattering processes have reached approximately 1.3×10^6 and 1.2×10^{10}, respectively. The numbers of available 4ph scattering processes are much larger than $LiCoO_2$[13], indicating that present calculations are sufficient to obtain an accurate κ_L.

The electronic band structure and deformation potentials are calculated using the PBE functional and employing 13×13×8 k-point meshes. We calculate the elastic constants C_{ij}, effective polar phonon frequency ω_{po}, static dielectric constants, high-frequency dielectric constants, and using DFPT, with the materials' parameters presented in Table S1 and S3. The precise band gap is obtained via the HSE06 functional[14]. To compute the electron relaxation time τ_e and electronic transport parameters, we re-calculate the electronic band structure using uniform 55×55×29 k-point grids, as implemented in the AMSET code[15]. The τ_e is calculated by including the fully anisotropic acoustic deformation potential (ADP) scattering, polar optical phonon (POP) scattering, ionized impurity (IMP) scattering, and grain boundary scattering.

Additionally, Table S2 also lists other mechanical property parameters of $XAgSe_2$ (X = Sc, Y) calculated by the Hill method[16]. The bulk modulus, Young's modulus, and shear modulus usually reflect the hardness and stiffness of a material. These mechanical parameters of $YAgSe_2$ are smaller than those of $ScAgSe_2$, indicating that the bonding strength decreases with increasing atomic number[17]. Furthermore, the ductility and brittleness of compounds can be evaluated by the Poisson's ratio[18] and Pugh's ratio[19]. If the former (or latter) is less than 0.26 (1.75), the compound is a brittle material; otherwise, it is a ductile material. It turns out that they are both brittle materials. In general, significant mechanical anisotropy may lead to microcracks in materials[20], so it is an important physical quantity to improve the durability of materials. We calculated the univerasl anisotropy index, and the results show that $YAgSe_2$ has strong anisotropy, indicating that $YAgSe_2$ has

large mechanical anisotropy properties.

Supplementary Figures

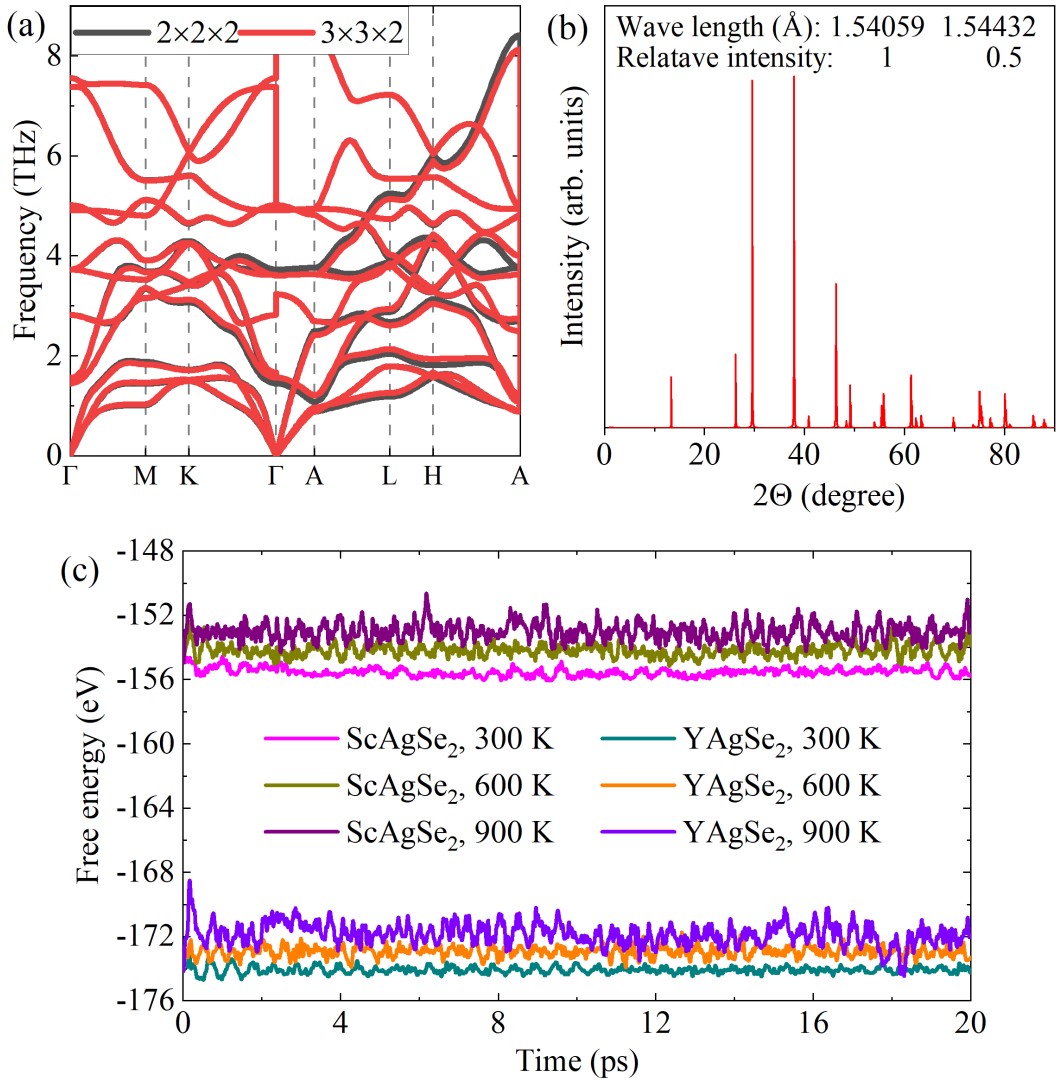

Fig. S1. (a) Comparison of harmonic phonon dispersion curves calculated using 2×2×2 and 3×3×2 supercells of $ScAgSe_2$. (b) The calculated diffractograms of $ScAgSe_2$. (c) The free energy as the function of time for $XAgSe_2$ (X = Sc, Y) at 300 K, 600 K and 900 K.

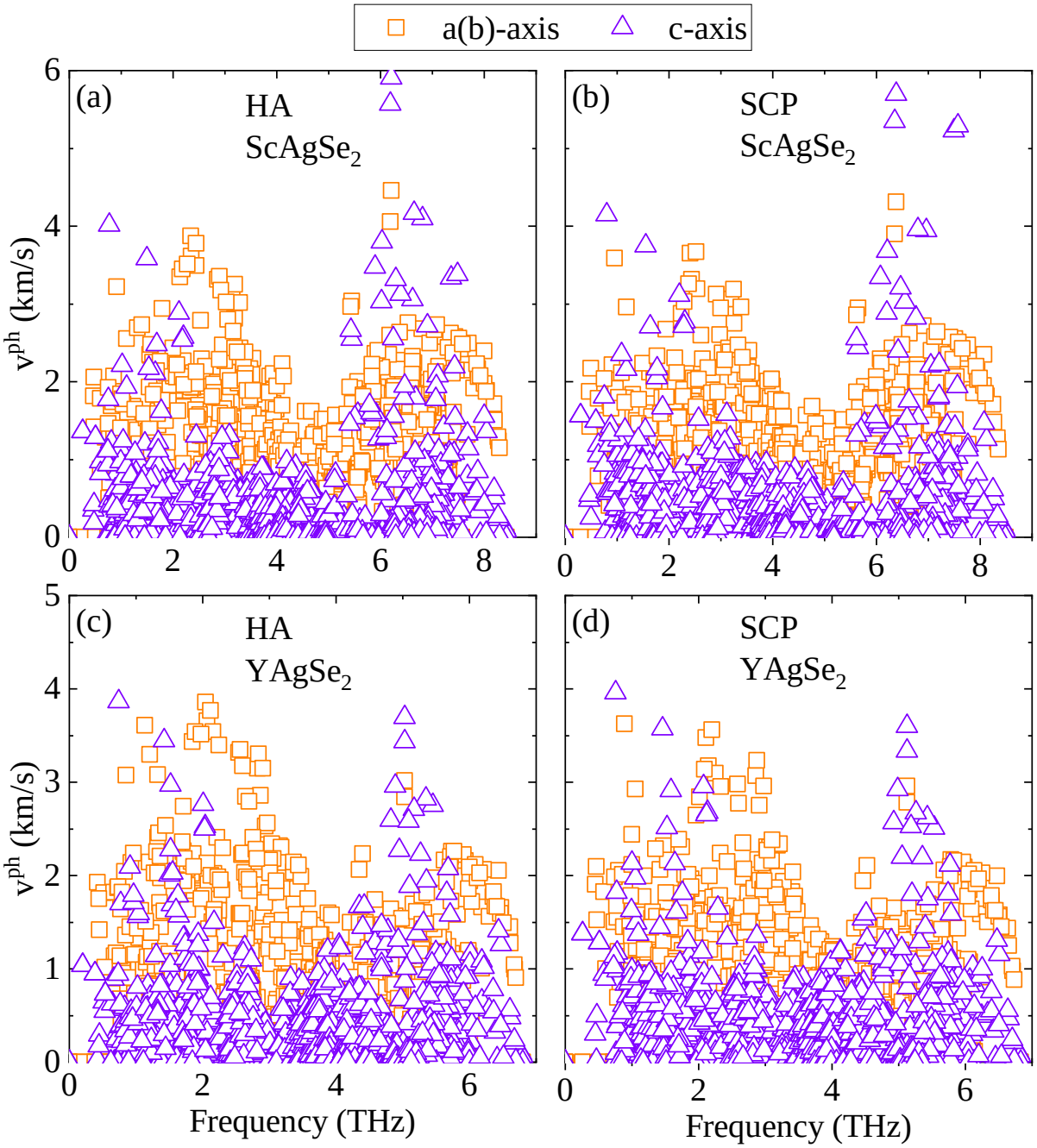

Fig. S2. The phonon group velocities (v^{ph}) of $ScAgSe_2$ and $YAgSe_2$ using HA and SCP methods. The result of SCP at 300 K.

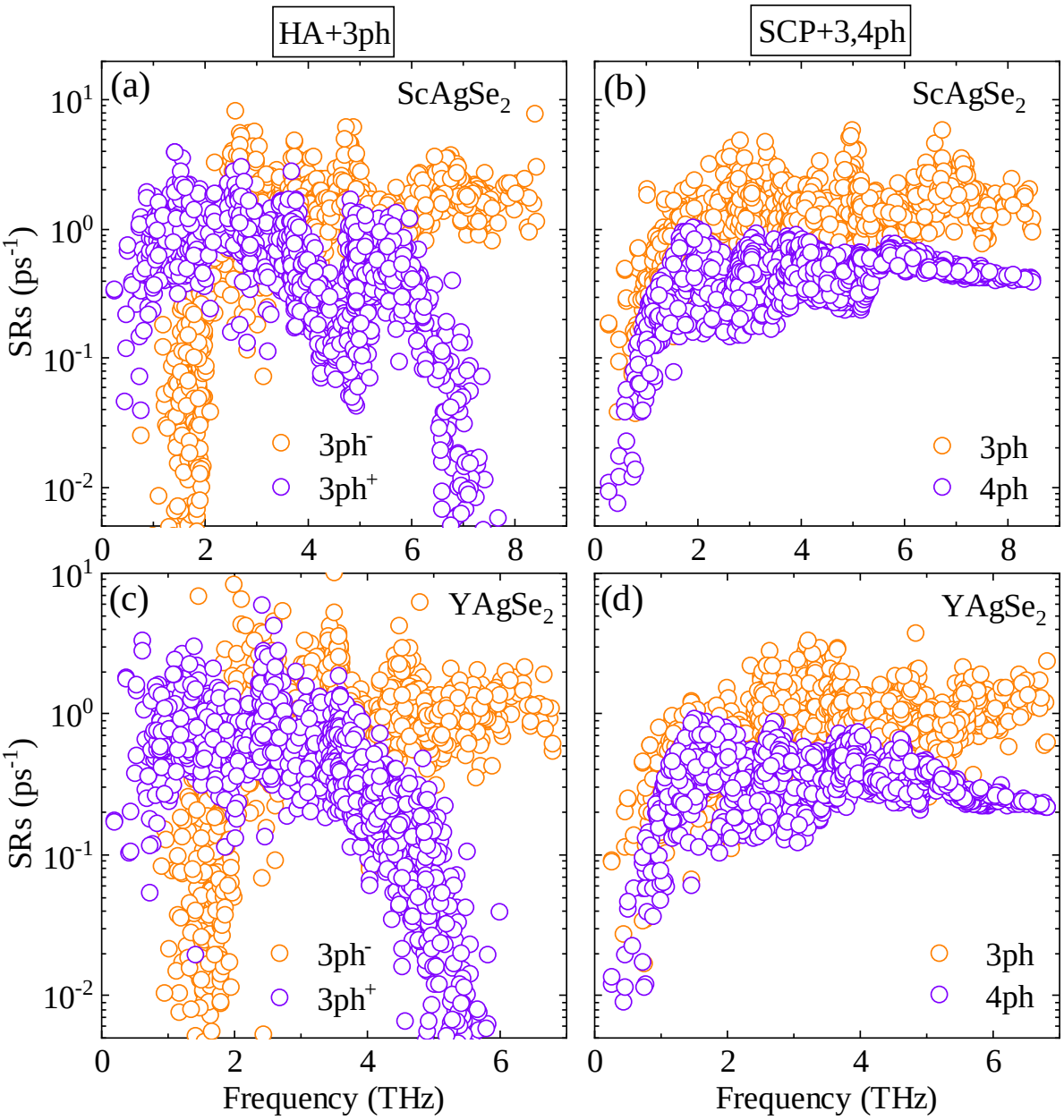

Fig. S3. Three-phonon scattering rates (SRs) of (a) $ScAgSe_2$ and (c) $YAgSe_2$ at 300 K, including emission ($3ph^-$) and absorption ($3ph^+$) processes. Three-phonon (3ph) and four-phonon (4ph) scattering rates of (b) $ScAgSe_2$ and (d) $YAgSe_2$ at 300 K.

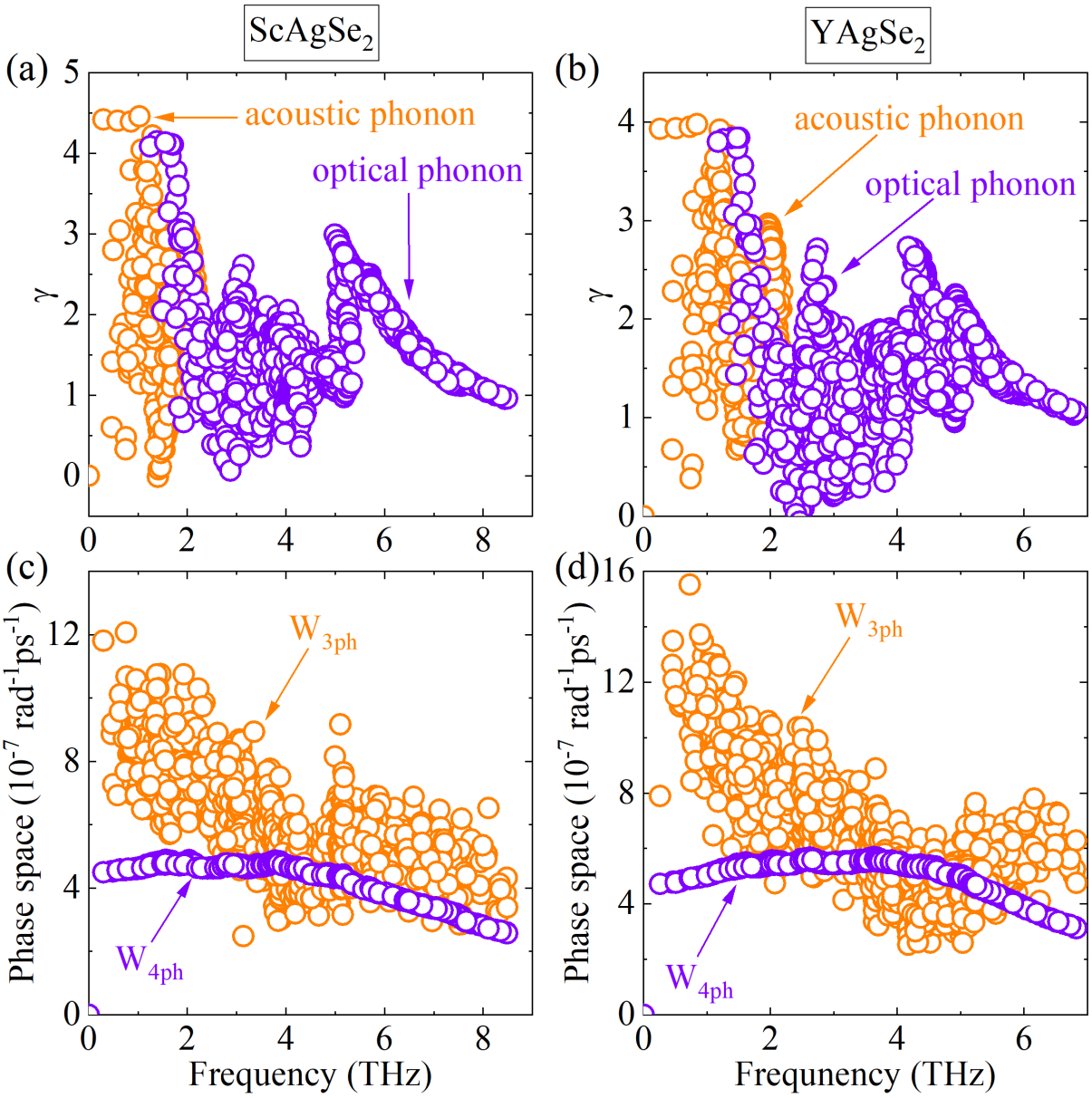

Fig. S4. The Grüneisen parameter (γ) as a function of the phonon frequency for for (a) $ScAgSe_2$ and (b) $YAgSe_2$.The 3ph and 4ph scattering phase space at 300 K for (c) $ScAgSe_2$ and (d) $YAgSe_2$.

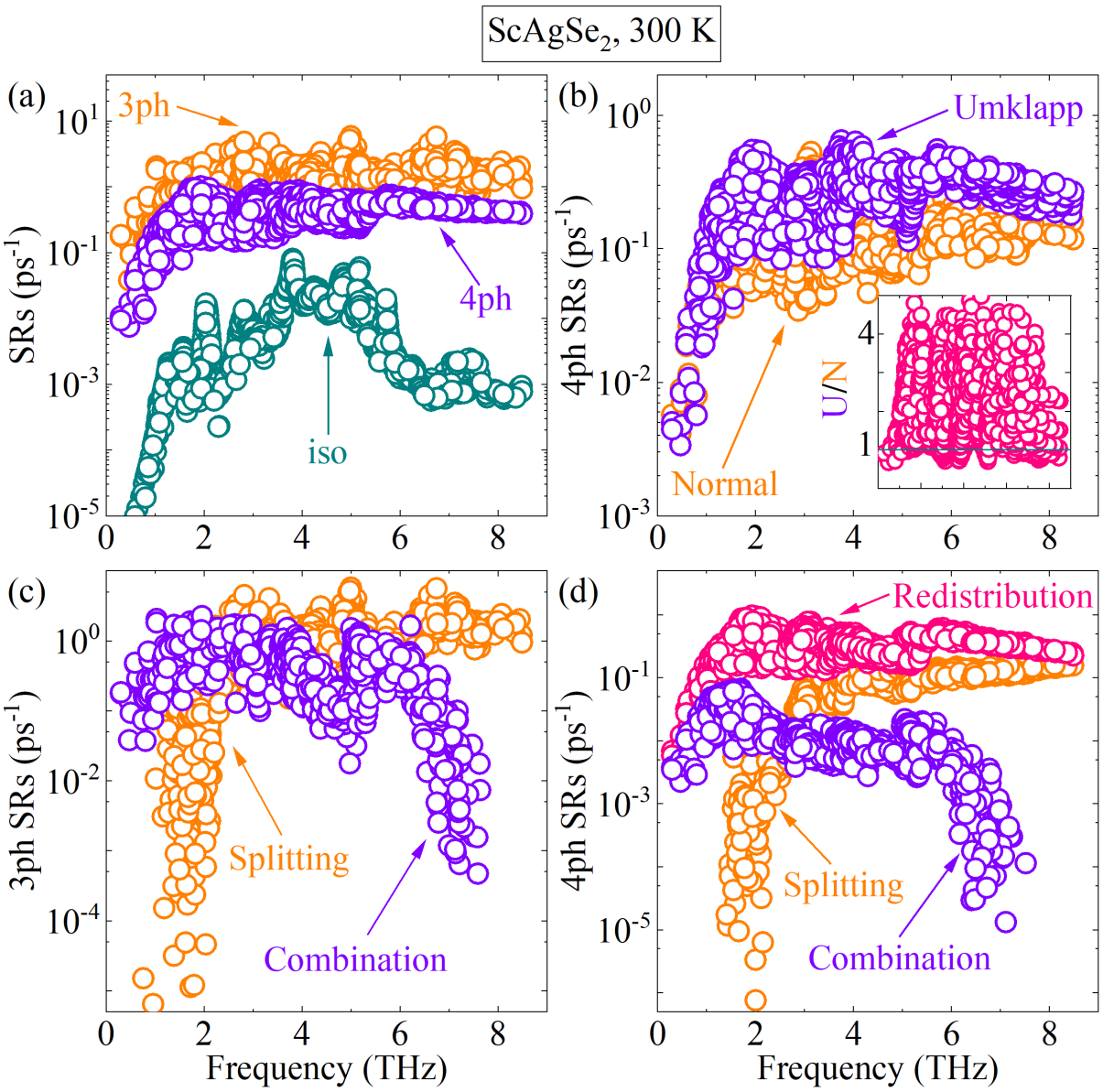

Fig. S5. (a) The 3ph, 4ph, and isotope scattering rates at 300 K of $ScAgSe_2$. (b) The 4ph scattering rates due to normal and umklapp processes. (c) Decomposed 3ph scattering rates into the splitting ($\lambda \rightarrow \lambda' + \lambda''$) and combination ($\lambda + \lambda' \rightarrow \lambda''$) processes. (d) Decomposed 4ph scattering rates into the splitting ($\lambda \rightarrow \lambda' + \lambda'' + \lambda'''$), redistribution ($\lambda + \lambda' \rightarrow \lambda'' + \lambda'''$), and combination ($\lambda + \lambda' + \lambda'' \rightarrow \lambda'''$) processes. All of the above results were obtained using SCP method.

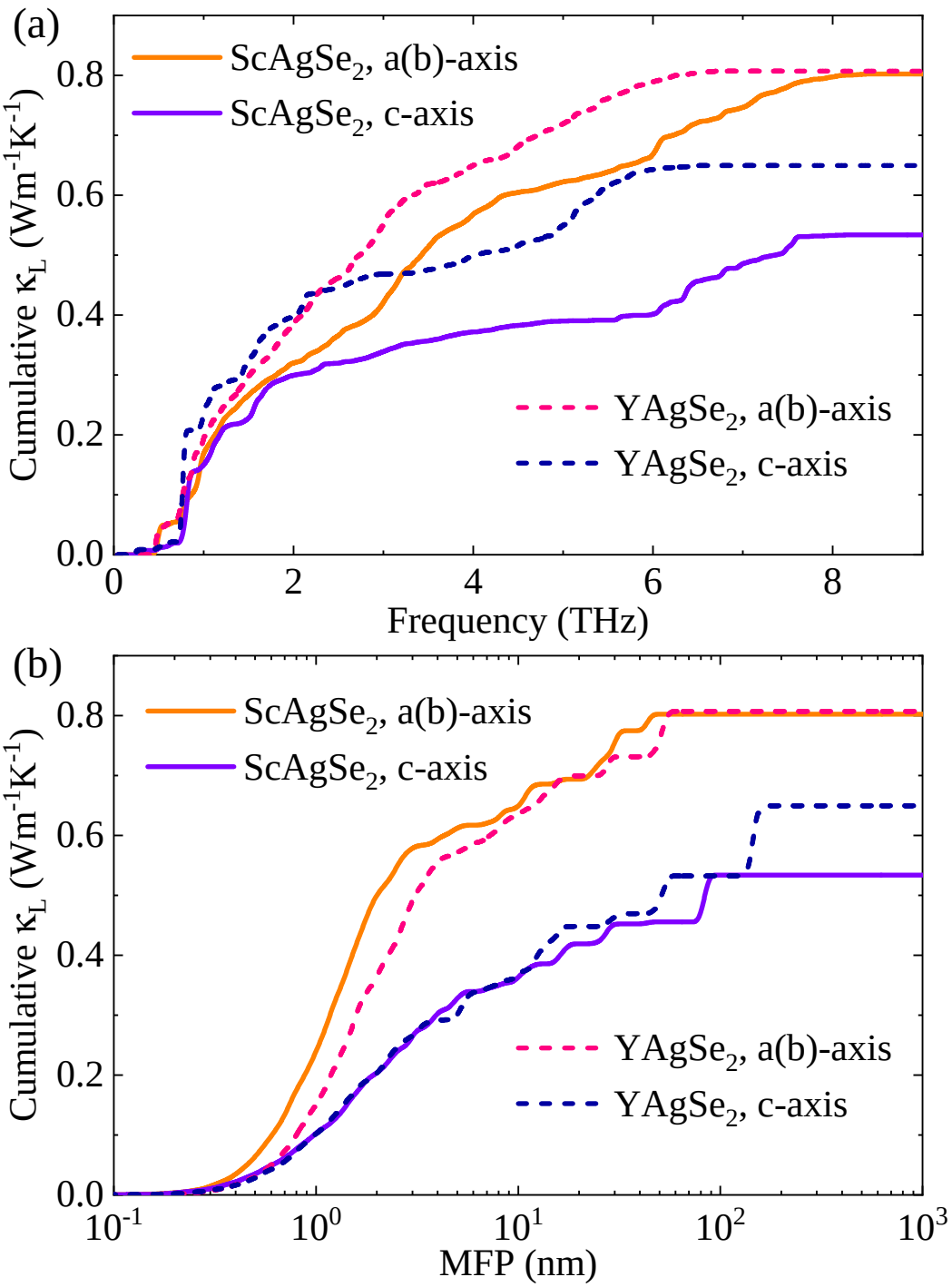

Fig. S6. (a) Cumulative κ_L as a function of phonon frequency for $XAgSe_2$ (X = Sc, Y). (b) Cumulative κ_L as a function of maximum mean free path (MFP).

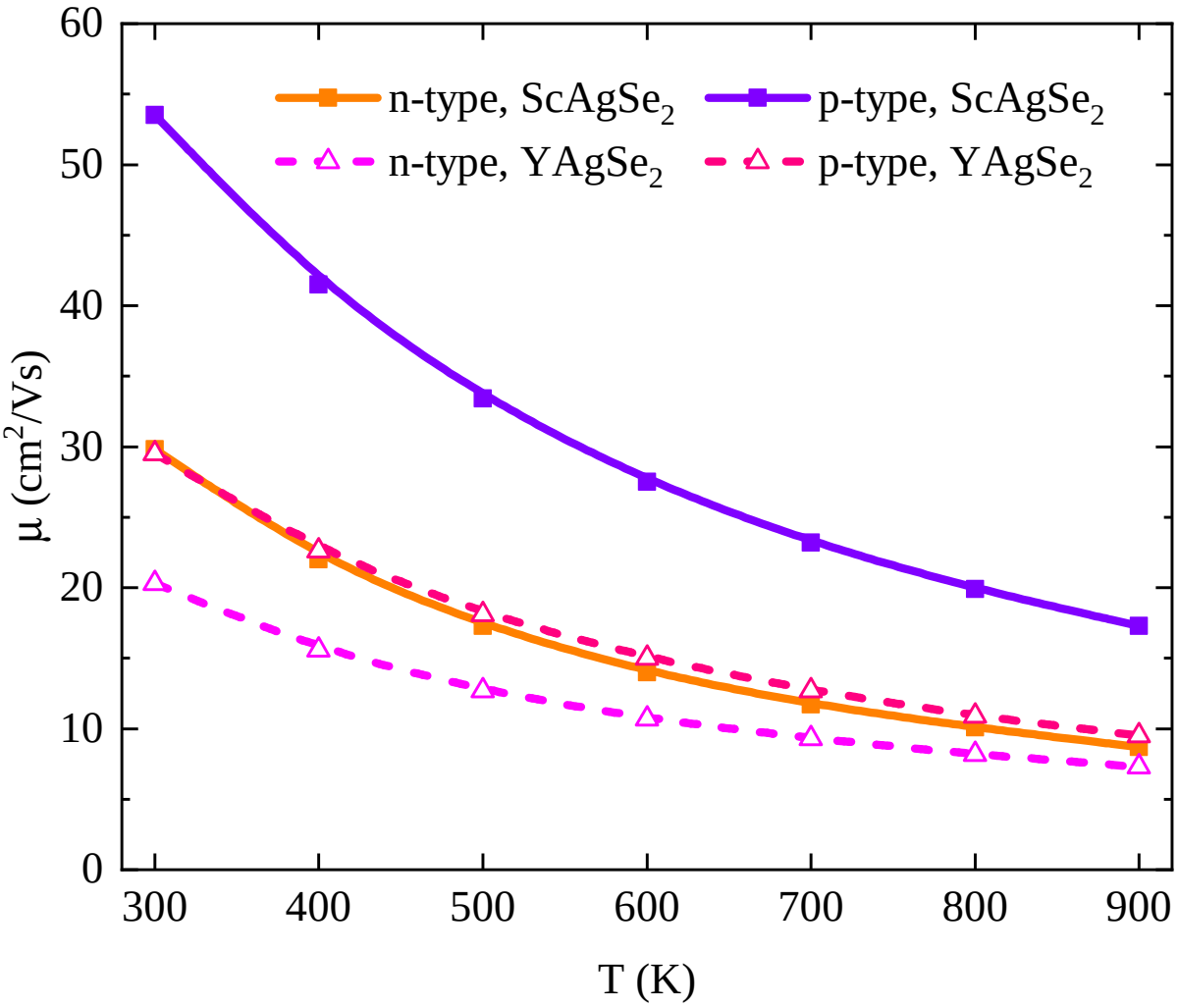

Fig. S7. (Color online). The calculated electron and hole mobilities (μ) as a function of temperature for $XAgSe_2$ (X = Sc, Y).

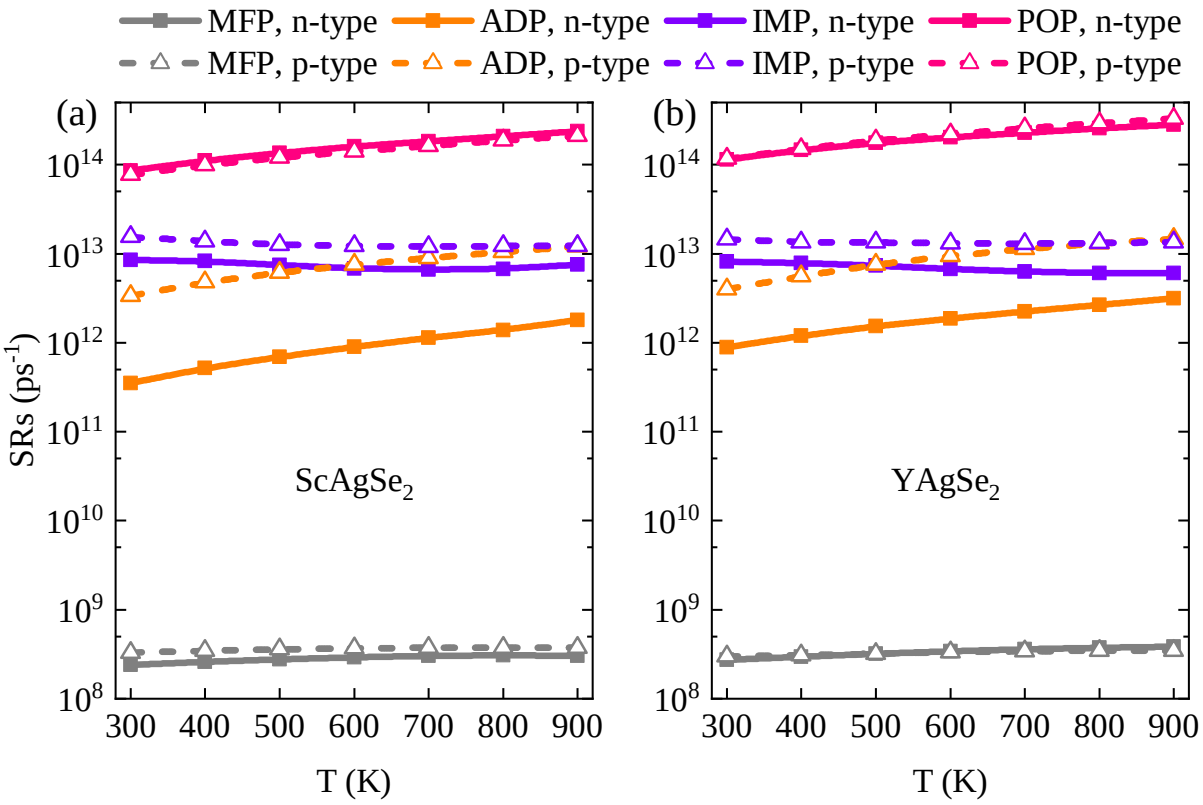

Fig. S8. (Color online). The electron scattering rates (SRs) as a function of temperature for (a) $ScAgSe_2$ and (b) $YAgSe_2$. The grey, orange, violet, and pink lines represent grain boundary (MFP) scattering, acoustic deformation potential (ADP) scattering, ionized impurity (IMP) scattering, and polar optical phonon (POP) scattering, respectively. The grain boundary size is set to 1 mm.

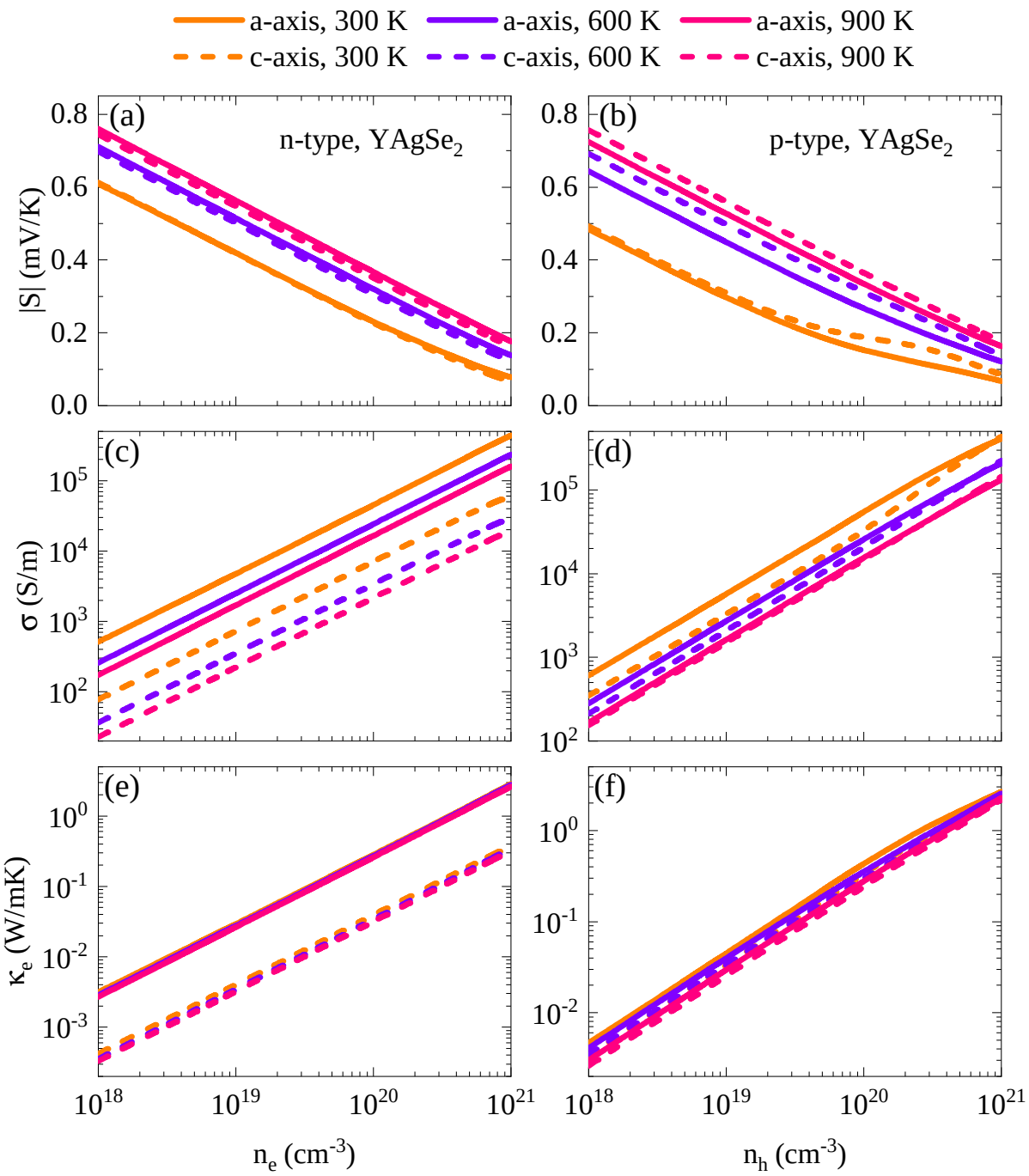

Fig. S9. (Color online). The calculated electron transport coefficients of n-type and p-type $YAgSe_2$, including the absolute value of the Seebeck coefficient $|S|$, electrical conductivity σ, and electrical thermal conductivity κ_e.

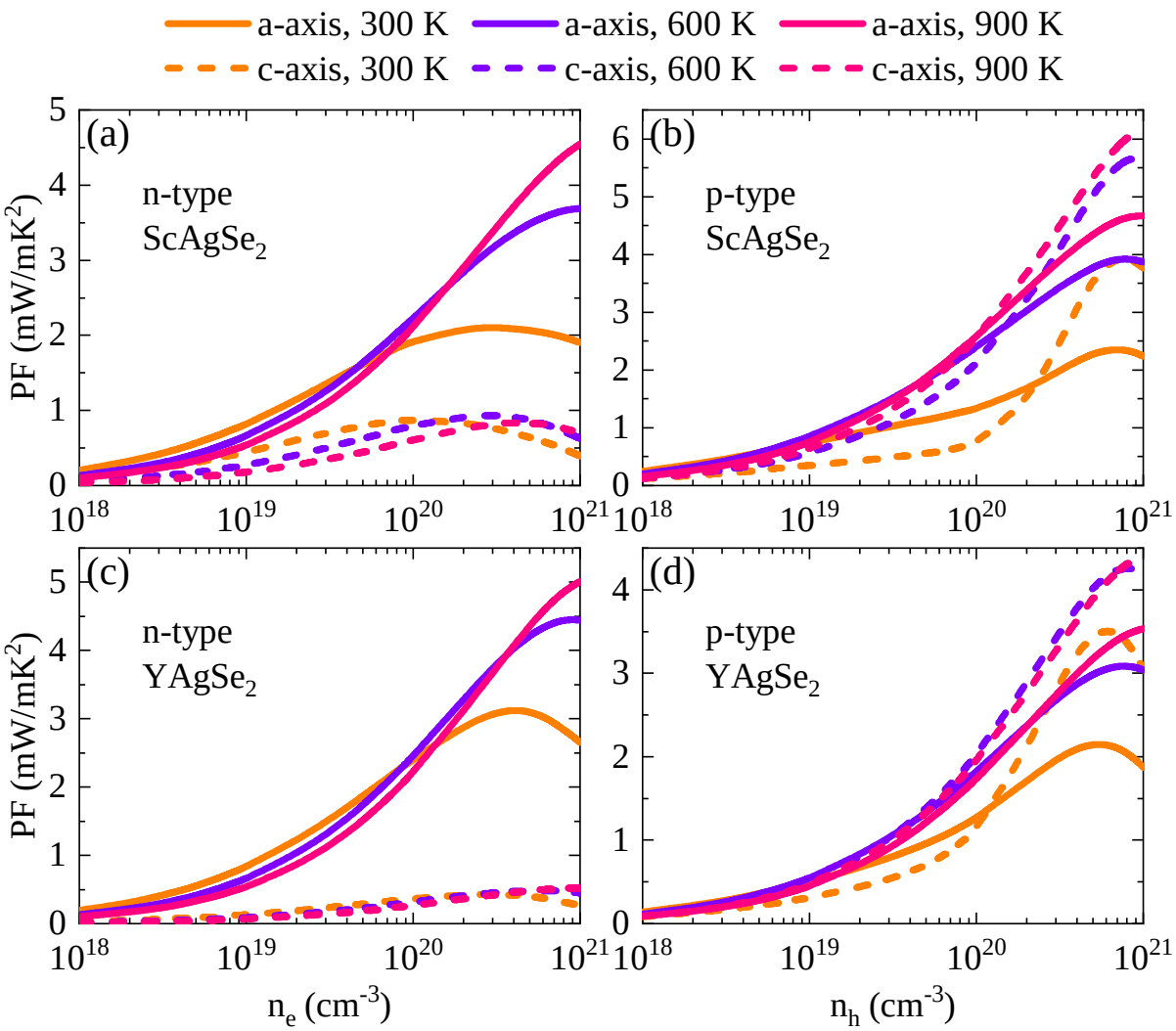

Fig. S10. (Color online). The calculated thermoelectric power factor (PF) as a function of carrier doping concentration for n-type and p-type $XAgSe_2$ (X = Sc, Y).

Supplementary Tables

TABLE S1. The calculated lattice constants ($a^{\rm opt}$ and $c^{\rm opt}$) (in Å) and irreducible elastic constants (C_{11}, C_{12}, C_{13}, C_{14}, C_{33}, C_{44}, and C_{66}) (in GPa) for the $ScAgSe_2$ and $YAgSe_2$, where have 6 independent components. The experimental lattice constants ($a^{\rm expt}$ and $c^{\rm expt}$) (in Å) quoted from Refs.[21] are listed for comparison.

material	$a^{\rm opt}$	$a^{\rm expt}$	$c^{\rm opt}$	$c^{\rm expt}$	C_{11}	C_{12}	C_{13}	C_{14}	C_{33}	C_{44}	C_{66}
$ScAgSe_2$	3.92	3.88	6.63	6.65	100.55	45.23	43.94	-3.45	99.33	10.90	27.66
$YAgSe_2$	4.09	-	6.71	-	93.54	39.92	35.52	-6.36	95.51	6.74	26.79

TABLE S2. The calculated dielectric tensor ϵ, Born effective charges Z^*, bulk modulus B (GPa), Young's modulus E (GPa), shear modulus G (GPa), isotropic poisson's ratio υ, Pugh's ratio B/G and universal elastic anisotropy A^U for the $ScAgSe_2$ and $YAgSe_2$.

material	ϵ	Z^*(X)	Z^*(Ag)	Z^*(Se)	B	E	G	υ	B/G	A^U
$ScAgSe_2$	12.29	4.12	1.65	2.89	62.95	51.32	18.81	0.36	3.35	1.35
$YAgSe_2$	9.96	3.96	1.65	2.80	56.06	40.39	14.63	0.38	3.83	4.97

TABLE S3. The calculated effective polar optical phonon frequency ω_{po} (THz), static dielectric constants ϵ_s, high-frequency dielectric constants ϵ_∞, Debye temperature Θ_D (K) and band gaps E_g (eV) for the $ScAgSe_2$ and $YAgSe_2$.

material	ω_{po}	ϵ_s	ϵ_∞	Θ_D	$E_g^{\rm PBE}$	$E_g^{\rm HSE06}$
$ScAgSe_2$	4.46	28.17	12.34	214.5	0.66	1.49
$YAgSe_2$	3.46	26.38	9.97	180.4	1.12	1.92

Supplementary References

---

* y.zhao@ytu.edu.cn

† zhdai@ytu.edu.cn

[1] G. Kresse and J. Furthmüller, Phys. Rev. B **54**, 11169 (1996).

[2] G. Kresse and D. Joubert, Phys. Rev. B **59**, 1758 (1999).

[3] J. P. Perdew, K. Burke, and M. Ernzerhof, Phys. Rev. Lett. **77**, 3865 (1996).

[4] S. Baroni, S. de Gironcoli, A. Dal Corso, and P. Giannozzi, Rev. Mod. Phys. **73**, 515 (2001).

[5] T. Tadano, Y. Gohda, and S. Tsuneyuki, Journal of Physics: Condensed Matter **26**, 225402 (2014).

[6] K. Esfarjani and H. T. Stokes, Phys. Rev. B **77**, 144112 (2008).

[7] F. Zhou, B. Sadigh, D. Åberg, Y. Xia, and V. Ozoliņš, Phys. Rev. B **100**, 184309 (2019).

[8] Y. Zhao, C. Lian, S. Zeng, Z. Dai, S. Meng, and J. Ni, Phys. Rev. B **101**, 184303 (2020).

[9] Z. Zeng, C. Zhang, Y. Xia, Z. Fan, C. Wolverton, and Y. Chen, Phys. Rev. B **103**, 224307 (2021).

[10] T. Tadano and S. Tsuneyuki, Phys. Rev. B **92**, 054301 (2015).

[11] T. Feng, L. Lindsay, and X. Ruan, Phys. Rev. B **96**, 161201 (2017).

[12] T. Feng and X. Ruan, Phys. Rev. B **93**, 045202 (2016).

[13] Z. Han, X. Yang, W. Li, T. Feng, and X. Ruan, Computer Physics Communications **270**, 108179 (2022).

[14] R. R. Pela, M. Marques, and L. K. Teles, Journal of Physics: Condensed Matter **27**, 505502 (2015).

[15] A. M. Ganose, J. Park, A. Faghaninia, R. Woods-Robinson, K. A. Persson, and A. Jain, Nature Communications **12**, 1 (2021).

[16] R. Hill, Proceedings of the Physical Society. Section A **65**, 349 (1952).

[17] K. Panda and K. R. Chandran, Acta Materialia **54**, 1641 (2006).

[18] J. Haines, J. Léger, and G. Bocquillon, Annual Review of Materials Research **31**, 1 (2001).

[19] S. Pugh, The London, Edinburgh, and Dublin Philosophical Magazine and Journal of Science **45**, 823 (1954).

[20] P. Ravindran, L. Fast, P. A. Korzhavyi, B. Johansson, J. Wills, and O. Eriksson, Journal of Applied Physics **84**, 4891 (1998).

[21] V. Shemet, L. Gulay, and I. Olekseyuk, Journal of Alloys and Compounds **426**, 186 (2006).